Polar vortex weakening and its impact on surface temperature in recent decades

Seong-Joong Kim & Hyesun Choi

Division of Atmospheric Sciences, Korea Polar Research Institute, Incheon, Republic of Korea

Abstract

The stratospheric polar vortex (SPV) weakening is linked to surface circulation changes. This study employs statistical analysis using reanalysis data to compare the anomalous SPV behaviour in the Northern (NH) and Southern (SH) hemispheres and its downward impacts on surface climate. The onset of annual SPV weakening occurs in mid-January and late September in the NH and SH hemispheres, respectively. Following the onset of SPV weakening, stratospheric polar cap height (PCH) anomalies were strongly correlated with tropospheric PCH anomalies. Significant cold anomalies were observed over Eurasia within 30 days after SPV weakening onset in the NH, whereas warming responses occurred in the SH 30–60 days after onset over Antarctica, except in the Antarctic Peninsula. These contrasting surface temperature responses to SPV weakening events in both hemispheres are the results of changes in the geopotential height in the troposphere, reminiscent of the change in geopotential height in the lower stratosphere, with a trough over Eurasia in the NH, and a higher height anomaly over East Antarctica in the SH. SPV changes have played a role in modulating surface climate via a downward influence on tropospheric circulation in recent decades. Even though they show a weakening trend in both hemispheres, SPV changes cannot fully explain long-term temperature trends. This is partially because SPV trends observed during the analysis period are relatively weak. This study enhances our understanding of the characteristics of the SPV coupled with troposphere circulation and can contribute to improved surface weather forecasting.

To access the supplementary material, please visit the article landing page

Introduction

The polar vortex is a planetary-scale westerly flow during the cold season that encircles the poles in the stratosphere (Manney et al. 2022) and connects the Arctic and Antarctic to mid-latitudes. In the NH, the weakening of the polar vortex often results in extremely cold weather across parts of Eurasia and North America in winter (Cohen, Screen et al. 2014; Kim et al. 2014; Kidston et al. 2015; Kretschmer, Cohen et al. 2018; Kretschmer, Coumou et al. 2018; Cohen et al. 2021; Kim & Choi 2021) via regional tropospheric jet stream variations (Manney et al. 2022), although not all weak polar vortices cause cold weather (Lehtonen & Karpechko 2016; Rao et al. 2020). Extremely weak polar vortex states are often associated with major SSWs, which are characterized by dramatic warming and weakening of the SPV and

reversal of circumpolar westerlies. When the polar vortex weakens, its morphology is distorted. Changes in the location and shape of the polar vortex, such as displacement and splitting during weak vortex states, including SSWs, often influence the timing and region of the cold spell in the NH (Lehtonen & Karpechko 2016; Huang et al. 2018; Choi et al. 2021; Zhang et al. 2022). Choi et al. (2021) observed that the SAT decreased markedly over central North America when the polar vortex changed from displacement- to split-type, likely because of the development of a high-pressure anomaly over the North Pacific, which is associated with the vertical and zonal propagation of planetary waves. Kim et al. (2014) observed that the delayed freeze-up of Arctic Sea ice during late fall and early winter, which mainly occurs in the Barents–Kara seas, weakens the SPV by activating planetary waves in the stratosphere, the downward

Citation: *Polar Research* 2024, *43*, 9723, http://dx.doi.org/10.33265/polar.v43.9723

propagation of which subsequently results in cold temperatures over Eurasia. However, in many numerical models, cold air outbreaks are underestimated because the simulated disruption of the polar vortex in the stratosphere is much smaller than the observed disruption (Cohen et al. 2020). Understanding the mechanism of polar vortex weakening and its downward propagation into the troposphere is critical for improving weather forecasts in the NH.

In Antarctica, polar vortices play an important role in driving climate variability (Thompson & Wallace 2000; Kwok & Comiso 2002; Thompson & Solomon 2002; Thompson et al. 2005; Kwon et al. 2020; Lim et al. 2021). Ozone depletion has been reported as a possible driver of SPV strengthening in the SH (Thompson & Solomon 2002; Polvani et al. 2011; Thompson et al. 2011; Sheshadri et al. 2014; Sun et al. 2014; Kidston et al. 2015; Ogawa et al. 2015; Hirano et al. 2016). In particular, from 1969 to 1998, the SPV in the SH became progressively stronger because of the depletion of stratospheric ozone concentration. Furthermore, the high index polarity in the SAM was reflected in the surface temperature as being colder than normal in most parts of Antarctica. However, this was not the case at the tip of the Antarctic Peninsula, on account of the reduced GPH in the upper troposphere over high southern latitudes (Thompson & Solomon 2002). At mid-latitudes, the stronger SPV due to ozone depletion is characterized by stronger easterly winds that lead to an increase in orographically induced precipitation during summer in eastern New Zealand and south-eastern Australia (Thompson et al. 2011). Thompson et al. (2011) showed that although ozone depletion is strongly linked to tropospheric temperature anomalies via SPV change, the underlying mechanism is unclear. Contrary to previous periods, since 2000, the SPV in the SH has led to more frequent weakening events that have induced significant cooling over the Antarctic Peninsula and warming over the rest of Antarctica (Kwon et al. 2020). In contrast to the NH, major SSWs have been rare in the SH, with only one major event—in 2002—over the past 60 years (Lim et al. 2021). Even though major SSWs are uncommon in the SH, weaker SPV events appear to influence the surface climate, as shown by Kwon et al. (2020), because SPV variations and their downward coupling to the troposphere seem to be critical drivers of variations in the SAM (Thompson & Wallace 2000). However, to date, only a few studies have examined downward coupling following a large SPV fluctuation in the SH (Thompson et al. 2005; Byrne & Shepherd 2018; Lim et al. 2018; Wang et al. 2019).

As discussed earlier in the text, the weakening of the polar vortex in the NH leads to extreme weather over mid-latitudes, whereas it is associated with surface temperature change over Antarctica in the SH. As the polar vortex appears to influence climate change locally in the Arctic and Antarctica and remotely at mid-latitudes in both hemispheres, investigating its behaviour in the context of climate change may improve our understanding of long-term temperature trends and their impacts in mid-latitudes. In this study, we investigated the behaviour of the polar vortex and characteristics of the SPV coupled with tropospheric circulation in recent decades and the underlying role of modulated polar vortices on surface climate change from 1979 to 2017.

Data and methods

ERA-Interim reanalysis data from the European Center for Medium-Range Weather Forecasts (Dee et al. 2011) were used to examine the mean and anomalies of SAT, sea level pressure, zonal wind, meridional wind, temperature and GPH, with a spatial resolution of 1.5° × 1.5° vertically from 1000 hPa to 1 hPa at 37 levels, from 1 January 1979 to 30 June 2018. Daily climatology values were calculated using daily means smoothed by a 31-day running mean between 1979 and 2017. All anomalies were calculated from their departures from the 31-day running mean. Monthly sea-ice cover from ERA-Interim was obtained from January 1979 to December 2017. Monthly SCE over Eurasia was downloaded from the Rutgers Global Snow Laboratory. The Eurasian SCE index is computed by determining the monthly mean of snow-covered grid points within the Eastern Hemisphere between 0°E and 180°E (Cohen et al. 2012).

Although the wind reversal method has been widely used to define extreme SPV weakening events, such as SSWs, multiple methods have been used to identify them in the NH and there is no standardized definition (Butler et al. 2015). As SPV weakening events identified using the zonal wind reversal diagnostic are rare in the SH, for simplicity and consistency we define weakened SPV events using PCH anomalies, as proposed by Kwon et al. (2020), for both hemispheres. A PCH anomaly is defined as a GPH anomaly averaged over a polar cap (65–90 degrees) and normalized by its temporal standard deviation during the analysis period at each pressure level. Therefore, a PCH anomaly of 1 indicates one standard deviation at a corresponding pressure level and is unitless. The date of onset of an SPV weakening event is defined as the first day when the PCH anomaly at 10 hPa exceeds the 95th percentile based on the entire analysis period, which corresponds to a PCH anomaly of 1.73 in the NH and 1.65 in the SH. If another onset occurred within 60 days of the first onset, only the first date was considered in the analysis, as outlined in a previous study

(Thompson & Solomon 2002). A positive PCH anomaly that was maintained for fewer than seven days following onset was identified as a temporarily large anomaly, and was therefore excluded from analyses of SPV weakening events (Kwon et al. 2020). We excluded SH stratospheric final warming events, which are defined as the final time when the zonal-mean zonal wind speed smoothed by a five-day running mean at 60°S and 50 hPa drops below 10 m s^{-1} between 1 July and 1 February of the following year (Black & Mcdaniel 2007). In the NH, they are defined as the date in which the direction of zonal-mean zonal wind at 64.5°N and 10 hPa changes from a westerly to an easterly wind and does not recover between 1 January and 31 May without any positive threshold value (Wei et al. 2007). Among the SPV weakening events classified earlier in the text, we analysed only robust SPV weakening events, defined as PCH anomalies at 10 hPa that were ≥ 2.8 for at least one day between onset and 60 days following onset, to focus on strong stratosphere–troposphere coupling events (Kwon et al. 2020). The PCH anomaly threshold value of 2.8 is higher than the 98th percentile for both hemispheres. We performed a two-sided Student's t-test to determine the statistical significance at the 95% confidence level. We used the SPVI, which is defined as the average PCH anomaly at 10 hPa in February in the NH and October in the SH, to investigate the relationship between the strength of the SPV and surface temperature.

We examined the fraction of trends in SAT anomaly in the high-latitude regions of the NH and SH that are linearly congruent with the SPV state. This was determined by regressing the detrended monthly SAT anomaly onto detrended SPVI and then multiplying the calculated regression coefficients by the SPVI trend for the 1979–2017 period.

Results

We first estimated the frequency of the SPV weakening events in both hemispheres since 1979, because the data are more reliable after satellite measurements. Applying the same definition of SPV weakening events to both hemispheres, we detected 22 and 15 SPV weakening events in the NH and SH, respectively (Table 1). The onset of SPV weakening in the NH ranged from 21 November (1987) to 5 March (2016), with a mean date of 17 January, and from 3 August (1988) to 28 October (1991), with a mean date of 22 September in the SH.

Since the beginning of the 21st century, changes in the long-term variability of the SPV state or factors related to the SPV state have been reported in the NH and SH. The increases in Arctic sea-ice loss and Eurasia SCE have been

Table 1. Onset dates of SPV weakening events in the NH and the SH. For the NH, the onset dates are identified by PCHA10 and the wind reversal method. When NH SPV weakening events and NH SSWs correspond to the same event, they are listed on the same line, even though the onset date might be slightly different. Dates in boldface indicate events that occurred after 2000.

Number	NH (PCHA10[a])		NH (U10 at 60°N[b])		SH (Kwon et al. 2020)	
	Year	Onset date	Year	Onset date	Year	Onset date
1	1980	28 Feb	1980	29 Feb	1979	02 Oct
2			1981	04 Mar		
3			1981	04 Dec		
4	1984	23 Feb	1984	24 Feb	1982	08 Oct
5	1984	28 Dec	1985	01 Jan	1988	03 Aug
6	1987	18 Jan	1987	23 Jan	1991	28 Oct
7	1987	21 Nov	1987	08 Dec	1992	30 Sep
8			1988	14 Mar		
9	1989	18 Feb	1989	21 Feb	**2000**	**10 Oct**
10	1992	12 Jan			**2002**	**15 Aug**
11	1993	30 Dec			**2003**	**12 Oct**
12	1997	21 Dec			**2004**	**26 Sep**
13	1998	13 Dec	1998	15 Dec	**2007**	**18 Sep**
14	1999	25 Feb	1999	26 Feb	**2009**	**14 Oct**
15			**2001**	**11 Feb**		
16	**2001**	**22 Dec**	**2001**	**30 Dec**	**2012**	**20 Aug**
17	**2003**	**16 Jan**	**2003**	**18 Jan**	**2013**	**18 Sep**
18	**2003**	**21 Dec**	**2004**	**05 Jan**	**2014**	**07 Oct**
19			**2005**	**13 Mar**		
20	**2006**	**05 Jan**	**2006**	**21 Jan**	**2017**	**22 Aug**
21			**2007**	**24 Feb**		
22	**2008**	**22 Feb**	**2008**	**22 Feb**		
23	**2009**	**21 Jan**	**2009**	**24 Jan**		
24	**2010**	**25 Jan**	**2010**	**09 Feb**		
25	**2013**	**05 Jan**	**2013**	**06 Jan**		
26	**2015**	**02 Jan**				
27	**2016**	**05 Mar**	**2016**	**05 Mar**		
28	**2017**	**30 Jan**				
29			**2018**	**12 Feb**		

[a]PCH anomalies at 10 hPa. [b]The wind reversal method.

observed since the year 2000 and are associated with the weakening of the SPV (Francis & Vavrus 2012; Jaiser et al. 2012; Cohen, Furtado et al. 2014; Kim et al. 2014). In the SH, around 2000, stratospheric ozone and near-surface circulation metrics, including the mid-latitude jet position and SAM index, showed a pause or slight reversal in trends (Solomon et al. 2016; Banerjee et al. 2020; Zambri et al. 2021). Kwon et al. (2020) confirmed that SH SPV weakening events have been observed more frequently since the year 2000. However, we found no differences in the frequency of SPV weakening events in the NH before versus after 2000 (Table 1). In the NH, SPV

weakening events occurred almost evenly throughout the cool months (November to March) before 2000, whereas after 2000, seven out of 11 events occurred in January. This implies that the probability of NH SPV weakening events has become concentrated over specific calendar months in recent decades.

On the basis of the 22 SPV weakening events in the NH listed in Table 1, Fig. 1a–b illustrates the vertical distribution of the composite values of PCH anomalies from the date of onset (day "0") ±90 days and for calendar months. In the NH, after the onset of SPV weakening events, positive PCH anomalies were observed in the upper stratosphere, showing a maximum value (3.8) at 1 hPa shortly after the onset date. The SPV weakening events and positive anomalies gradually descended to the lower stratosphere and troposphere and lasted for approximately 60 days in the upper troposphere. Positive anomalies within the troposphere and near the surface became significant shortly after onset. The average date of onset for SPV weakening events was 17 January (Table 1), and positive PCH anomalies occurred from the end of December until mid-March in the stratosphere and troposphere, although positive values were relatively small for all months (Fig. 1b). Figure 1c illustrates the trend in PCH anomalies calculated for each calendar day and for each vertical level from 1 July 1979 to 30 June 2018 and is similar to Figure 8a by Cohen et al (2018), which was calculated for the 1990–2016 time period using different reanalysis data than we used for the study that we report here. Although significant signals were confined to a narrow period, stratospheric PCH anomalies exhibited an increasing trend over the time period analysed, especially in February, which is consistent with the more frequent occurrences of SPV weakening events during the mid-winter observed after 2000.

Figure 2 illustrates a composite of PCH anomalies and trends in the SH. Figure 2a illustrates that positive PCH anomalies persisted for over three months after the date of onset in the stratosphere and approximately 50–80 days in the troposphere. The maximum PCH anomaly was approximately 2.9 at 1 hPa shortly after the date of onset in the SH, which was smaller than that in the NH. In contrast to the NH, where SPV weakening events occurred over a broad temporal range, such events tended to occur at similar times of the year in the SH—about 22 September—and exhibited similar evolutions. Therefore, the composite mean results are less sensitive to the reference timings in the analysis, such as the onset date (day 0) for events or calendar date (July 1) when events occurred (Fig. 2a, b; Kwon et al. 2020). The phase-locking characteristics of SPV weakening events in the SH differ considerably from those in the NH (Charlton & Polvani 2007). Figure 2c illustrates the linear trend of PCH

anomalies in the SH. As indicated by Kwon et al. (2020), a PCH anomaly in the SH increases with time, indicating a weakening of the SPV. That study identified an increasing PCH trend in the stratosphere during September, although the significant signal was limited to a short period, and in the troposphere during October and November. As SPV weakening events have been observed to occur more frequently since the 2000s (Table 1), changes in SPV weakening events in recent decades have likely contributed significantly to the recent trend toward a low SAM (positive PCH anomaly). In contrast to the NH, the increasing trend of PCH anomalies in the lower stratosphere was limited to a few months in the SH.

To identify the stratosphere–troposphere coupling based on a monthly timescale (downward impact of SPV weakening events), we examined the relationship between PCH anomalies at 500 hPa (PCHA500) for three different periods and PCH anomalies at 10 hPa averaged over 30 days after the onset of an SPV weakening event (PCHA10; Supplementary Fig. S1). A positive PCH anomaly indicates a negative annular mode (Thompson & Solomon 2002). The correlation coefficients are not significant at the 95% confidence level, indicating that the relationship between stratospheric and tropospheric circulation may be weak or nonlinear. Nevertheless, the negative polarity of tropospheric circulation (positive PCHA500) occurred more frequently during specific periods. For example, in the NH, during the early period up to 30 days after onset, a more frequent (15 out of 22) negative Northern Annular Mode occurred, but in the SH, a negative SAM occurred more frequently (12 out of 15) during the late period 60 days after the onset of SPV weakening (Table 2). This is further confirmed through the composite mean value of PCHA500, shown in Supplementary Fig. S1. The positive values of PCHA500 are only statistically significant in the NH from days 0 to 30, and in the SH from day 30 onwards. The robust mean values show a tendency for more frequent occurrences of negative annular modes in the NH during the first 30 days and in the SH after 30 days.

Subsequently, we examined how SPV weakening events influence surface temperature. Figure 3 illustrates the responses of SAT at 2 m to SPV weakening events for three months after the date of onset. In the NH, the SAT became significantly colder over Eurasia during the first 30 days after onset; however, the degree of response was mitigated on later days. Significant warm SAT anomalies over north-western North America and cold SAT anomalies over north-eastern North America were identified during days 0–30. Compared to Eurasia, North American cooling at high latitudes was less robust for the period analysed, showing insignificant fluctuations behaviour. This suggests that the
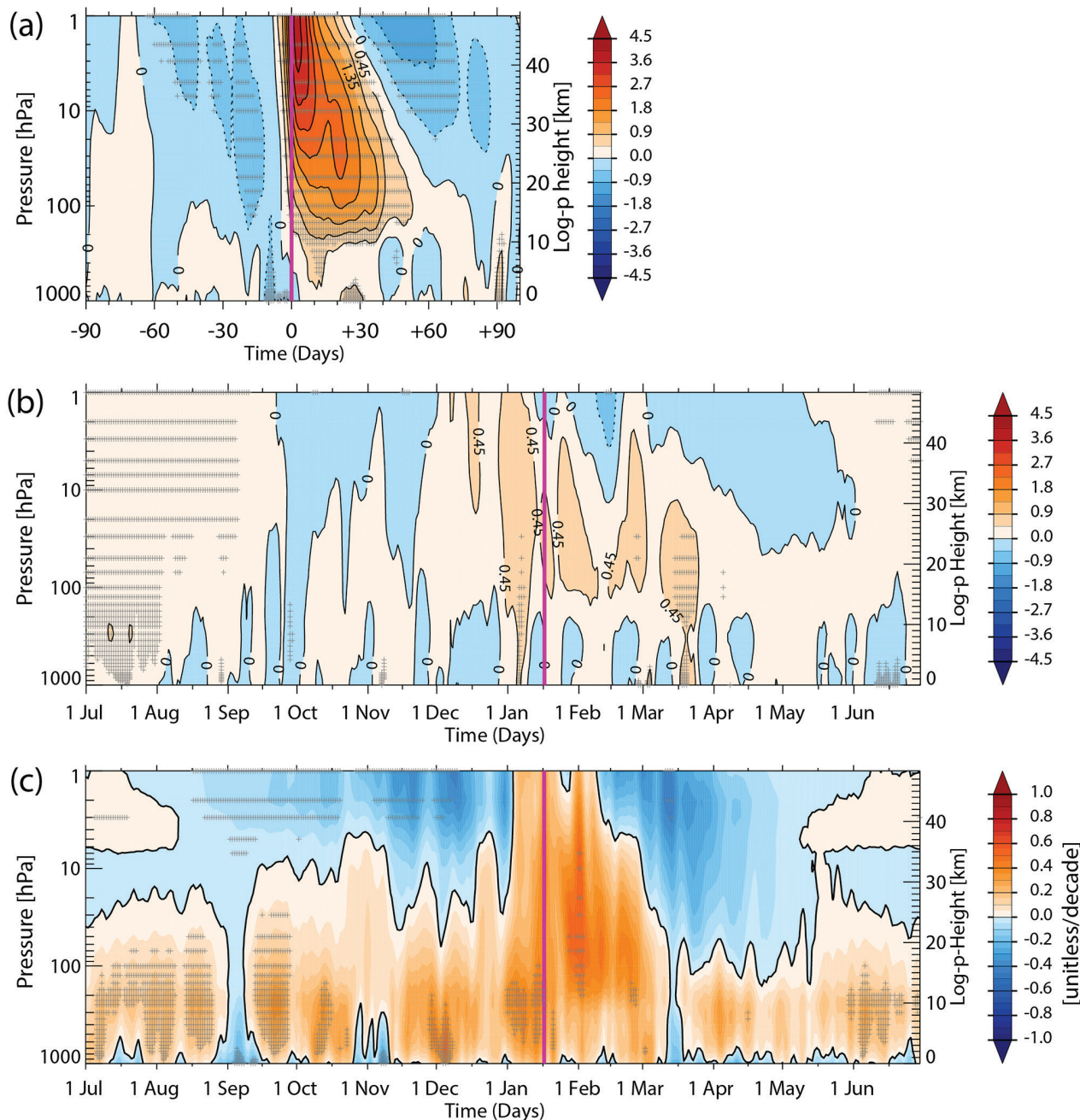
Fig. 1 (a) Composite of PCH anomalies based on onset date for SPV weakening events in the NH. (b) Same as (a) but based on 1 July of years corresponding to SPV weakening events. (c) Linear trends of PCH anomalies calculated for each calendar day and for each vertical level from 1 July 1979 to 30 June 2018. Grey crosses indicate statistically significant regions at the 95% confidence level. The pink vertical line indicates the onset date (day 0) in (a) and mean onset date (17 January) in (b) and (c).

impact of SPV weakening events on SAT might be particularly important in high-latitude Eurasia. The differences in surface temperature responses between Eurasia and North America are consistent with previous studies, despite the use of different detecting methods for SPV weakening events and a different data set (Kretschmer, Cohen et al. 2018; Huang et al. 2021). In the SH, the responses were more significant 30 or more days after onset. Between 30 and 60 days after onset, SAT became significantly warmer over Antarctica, except over the Antarctic Peninsula, and this feature of surface temperature response persisted until 90 days after onset.
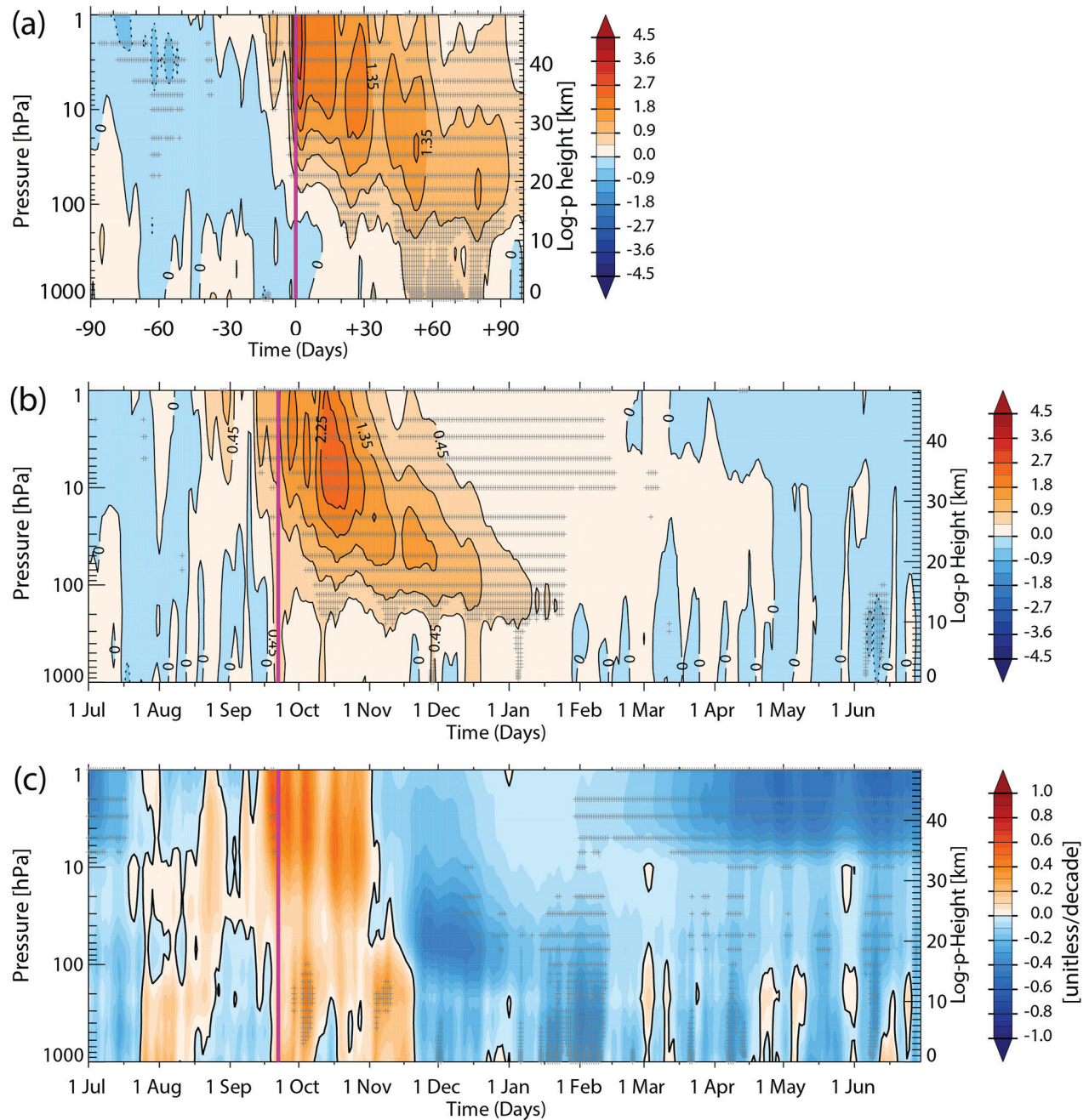
Fig. 2 (a) Composite of PCH anomalies based on onset date for SPV weakening events in the SH. (b) Same as (a) but based on 1 July of years corresponding to SPV weakening events. (c) Linear trends of PCH anomalies calculated for each calendar day and for each vertical level from 1 July 1979 to 30 June 2018. Grey crosses indicate statistically significant regions at the 95% confidence level. The pink vertical line indicates the onset date (day 0) in (a) and mean onset date (22 September) in (b) and (c). The illustration is a modified version of figure 1 by Kwon et al. (2020).

The surface temperature response to SPV weakening events is related to atmospheric circulation in the troposphere, which appears to be influenced by mass change in the stratosphere. Figure 4 illustrates GPH anomalies at 10, 100 and 500 hPa for the first 90 days after the onset of SPV weakening events. During the early period (0–30 days), lower height anomalies occurred over Eurasia and north-eastern North America, consistent with the colder anomalies in the surface temperature responses mentioned earlier in the text. During this period, higher height anomalies occurred over the North Atlantic and North Pacific, including Alaska. The lower height

Table 2. Number of positive PCH anomalies at 500 hPa (PCHA500) averaged over three different periods (days 0–30, 30–60, and 60–90) following the onset date of SPV weakening events in each hemisphere. Numbers in parentheses represent total number of SPV weakening events based on PCH anomalies that occurred during the analysis period, as shown in Table 1.

|	Days 0–30	Days 30–60	Days 60–90
NH	15 (22)	10 (22)	13 (22)
SH	7 (15)	9 (15)	12 (15)

anomalies in the troposphere over Eurasia and north-eastern North America and the higher height anomalies over the North Atlantic and North Pacific can be traced to the lower stratosphere (100 hPa level), where similar changes in GPH anomalies occurred. The barotropic feature between the lower stratosphere and troposphere implies that the stratospheric circulation during SPV weakening

events is coupled with the tropospheric circulation, consistent with results reported in a previous study (Woo et al. 2015). In the upper stratosphere, higher height anomalies were observed over the entire Arctic; however, no peculiar signature was observed for anomalous changes in the lower levels. From 30 to 60 days after onset, GPH anomalies in the troposphere were smaller than those of the earlier period over Eurasia, although lower height anomalies persisted. The mitigated GPH anomalies from 30 days onward were associated with the mitigated anomalies at upper levels in the stratosphere, where positive height anomalies over the Arctic were smaller than those in the earlier period. After 60 days, significant positive anomalies were no longer visible over the Arctic in the stratosphere and no traces were observed in the troposphere.

In contrast to the NH, SH GPH anomalies in the troposphere were not prominent in the first 30 days (Fig. 5).
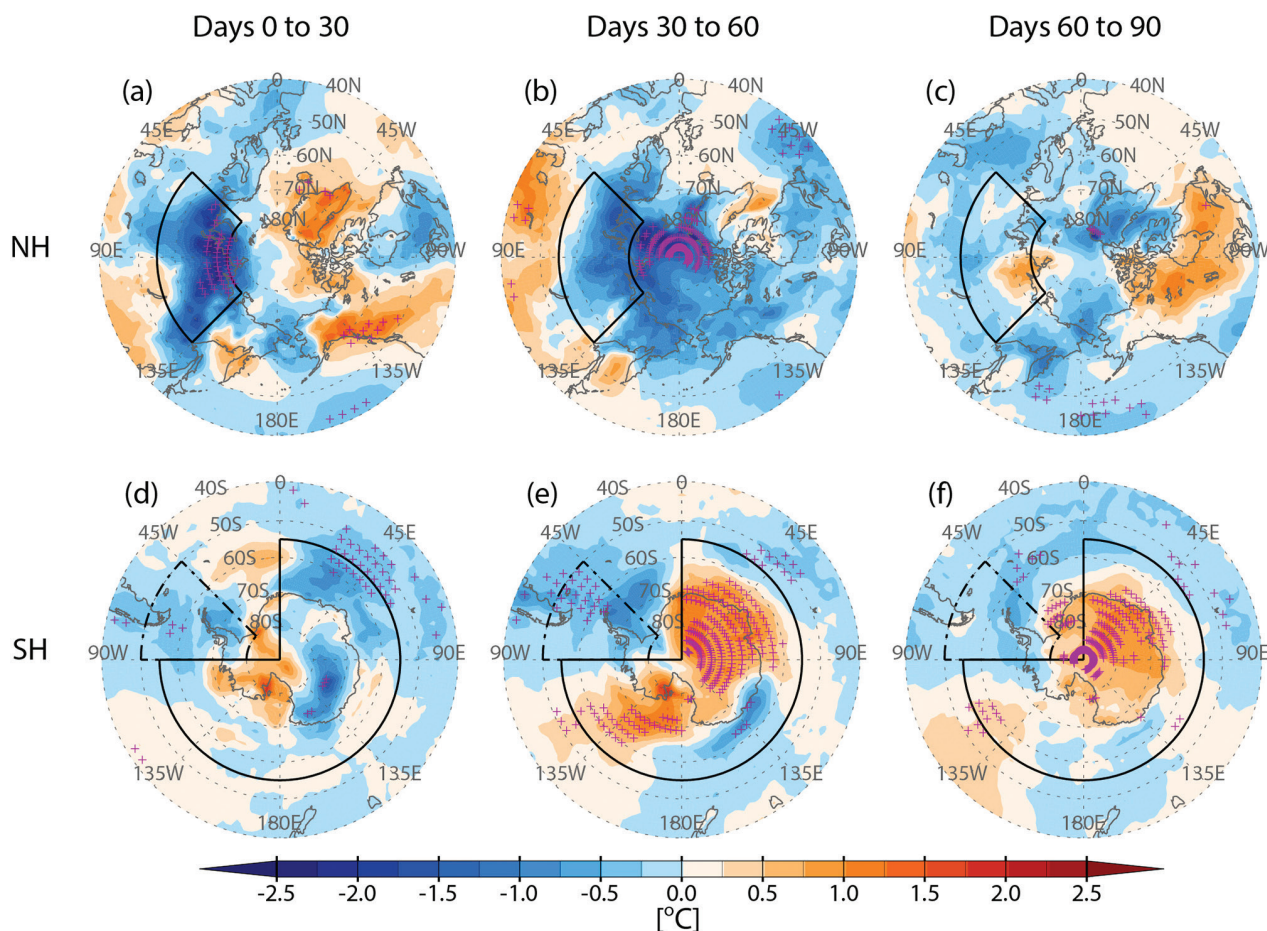

Fig. 3 SAT anomalies averaged over three different periods after the onset date of SPV weakening events in the (a–c) NH and (d–f) SH. Results are shown for (a, d) days 0–30, (b, e) days 30–60 and (c, f) days 60–90. Pink crosses indicate significant values at the 95% confidence level. Black solid boxes in (a–c) mark the Eurasia region (45°E–135°E, 55°N–75°N), while black dashed-dotted and black solid boxes in (d–f) indicate the Antarctic Peninsula region (270°E–315°E, 50°S–80°S) and the rest of Antarctica (0°E–270°E, 55°S–90°S), respectively.
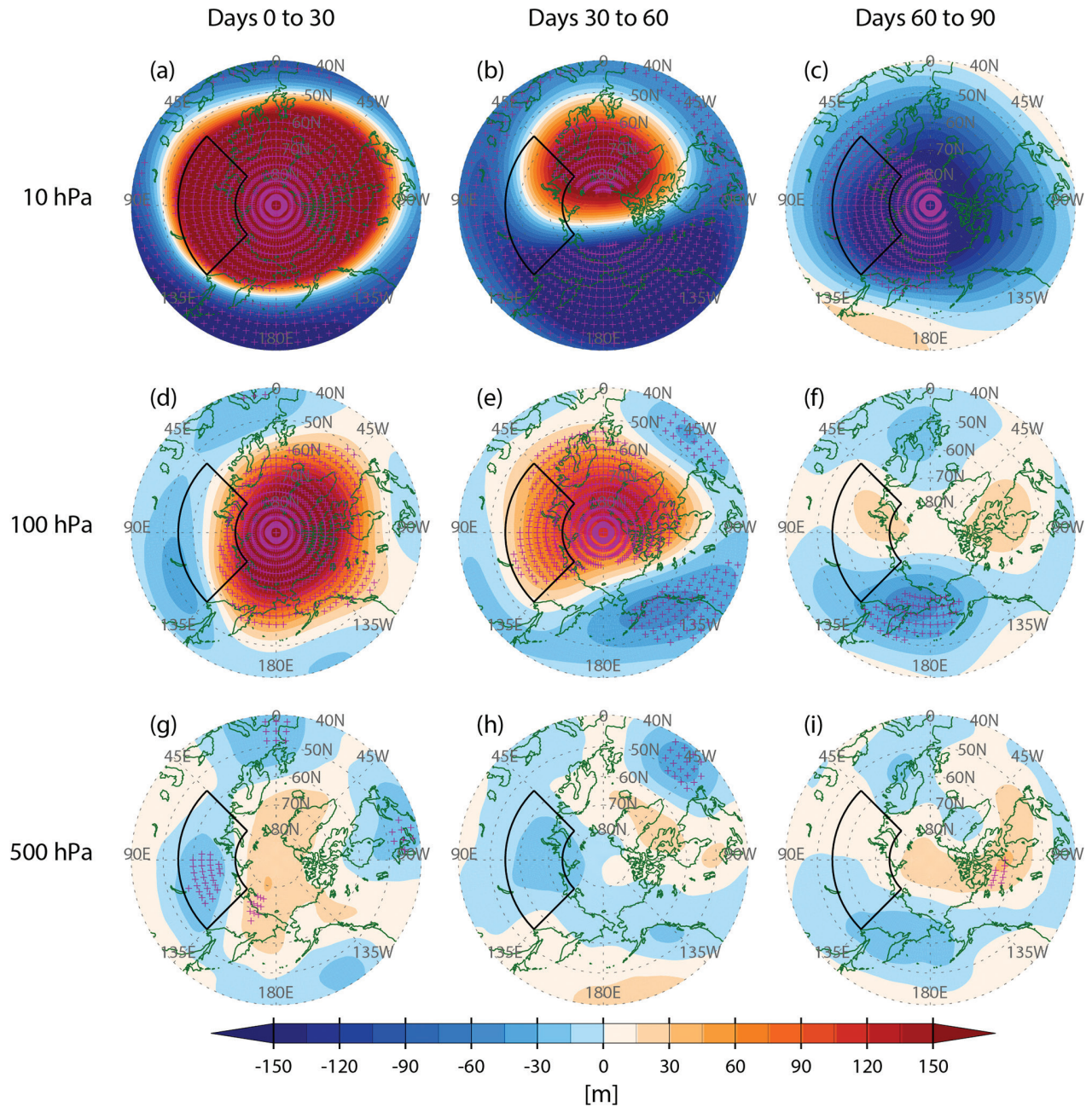
Fig. 4 GPH anomalies after the onset date of SPV weakening events in the NH. Results are shown at (a–c) 10 hPa, (d–f) 100 hPa and (g–i) 500 hPa, averaged (a, d, g) from days 0–30, (b, e, h) 30–60 and (c, f, i) 60–90. Pink crosses indicate significant values at the 95% confidence level. Black solid boxes mark the Eurasia region (45°E–135°E, 55°N–75°N).

The strongest positive anomalies occurred in the upper stratosphere, indicating slower propagation to the troposphere compared to that in the NH, which was also observed in the vertical section of the PCH anomalies (Fig. 2). From days 30 to 60, GPH anomalies markedly increased over East Antarctica and the Amundsen/ Bellinghausen sector of the Southern Ocean. The change

in GPH anomalies in the troposphere during this period is reminiscent of that in the lower stratosphere, where the largest positive anomalies occurred, particularly over the Amundsen–Bellinghausen seas and Indian Ocean sectors. Sixty days after onset, positive GPH anomalies centred over the eastern Antarctic sector were observed in the troposphere, reminiscent of those in the lower
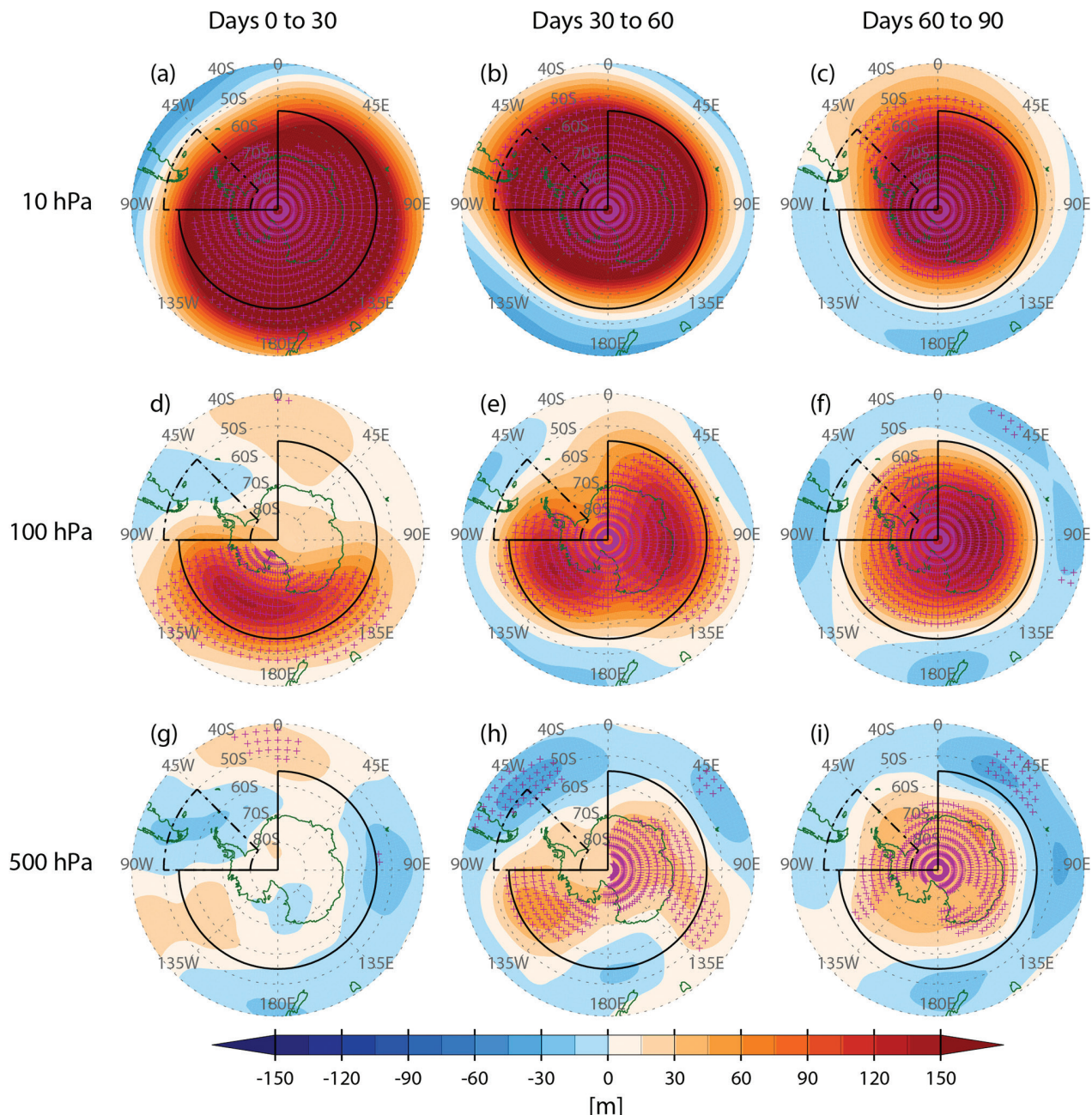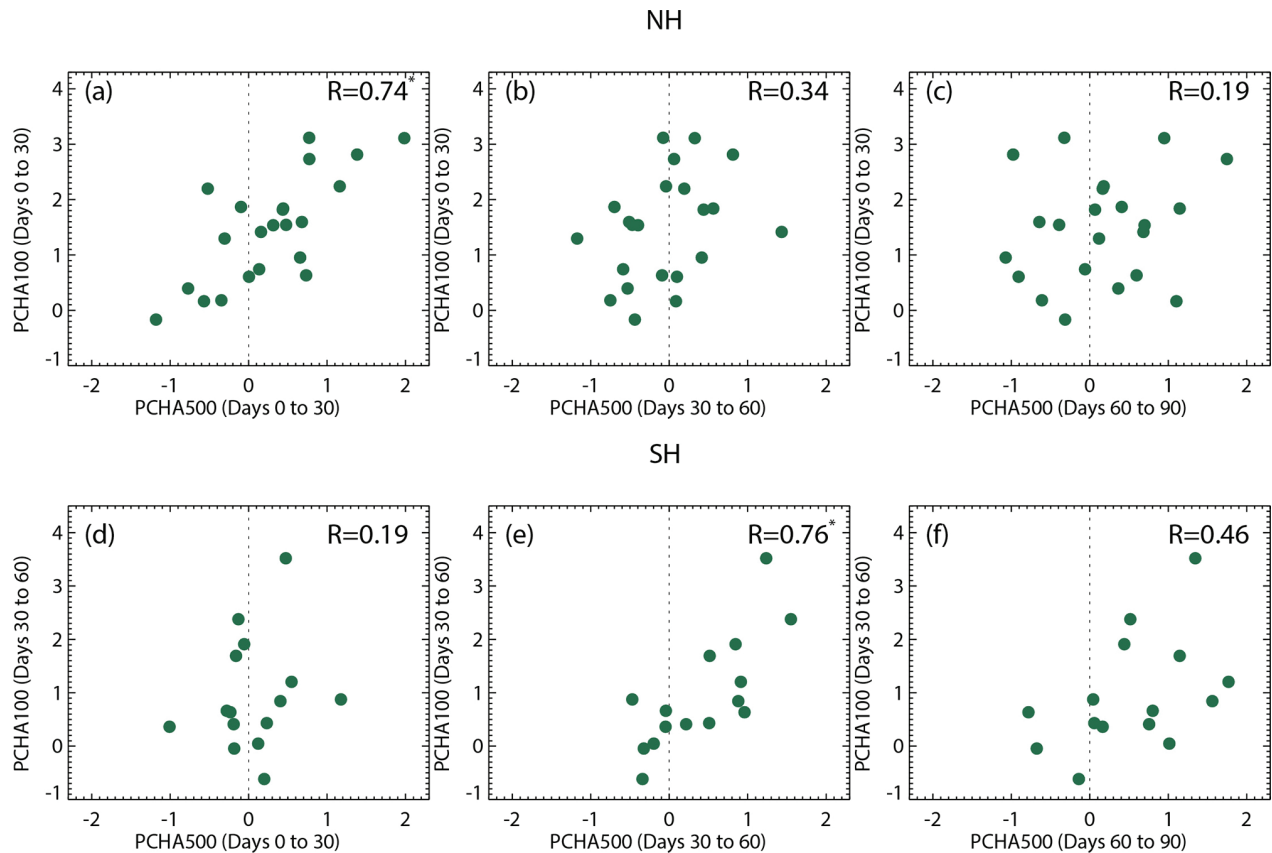
Fig. 5 GPH anomalies after the onset date of SPV weakening events in the SH. Results are shown at (a–c) 10 hPa, (d–f) 100 hPa and (g–i) 500 hPa, averaged (a, d, g) from days 0–30, (b, e, h) 30–60 and (c, f, i) 60–90. Pink crosses indicate significant values at the 95% confidence level. Black dashed-dotted and black solid boxes indicate the Antarctic Peninsula region (270°E–315°E, 50°S–80°S) and the rest of Antarctica (0°E–270°E, 55°S–90°S), respectively.

stratosphere. The higher height anomalies in the east and west Antarctic sectors were associated with warm anomalies at the surface (Fig. 3). In terms of hemispheric scale, from days 0 to 30 in the NH (Fig. 4) and from day 30 to 90 in the SH (Fig. 5), there were positive anomalies over the polar region and negative anomalies in the mid-latitudes. This is consistent with the frequent occurrence of

negative annular modes in the troposphere (positive PCHA500) during each period (Supplementary Fig. S1).

The spatial pattern of tropospheric GPH anomalies in both hemispheres was more similar to the lower stratosphere than the upper stratosphere (Figs. 4d, g, 5e, h). This is clearly illustrated in Fig. 6, which is the same as Supplementary Fig. S1, but shows PCH anomalies at

NH

SH

Fig. 6 (a–c) Scatterplots of PCH anomalies at 100 hPa (PCHA100) averaged over days 0–30 and at 500 hPa (PCHA500) averaged over three different periods after the onset date of SPV weakening events in the NH. (d–f) Same as (a–c) but showing PCHA100 averaged over days 30–60 and PCHA500 averaged over three different periods after the onset date of SPV weakening events in the SH. Results are shown for (a, d) days 0–30, (b, e) days 30–60 and (c, f) days 60–90. A correlation coefficient (R) between PCHA100 and PCHA500 is shown in the upper corner of each panel. Asterisks indicate a statistically significant value at the 95% confidence level.

100 hPa (PCHA100) averaged over days 0–30 in the NH and days 30–60 in the SH. The significant correlation coefficients (Fig. 6a, e) indicate that the relationship between lower stratospheric and tropospheric circulation is robust and linear.

We further examined the relationship between the circulation and SAT variations related to SPV weakening events (Supplementary Figs. S2, S3). On the basis of the major regions associated with SPV weakening events, such as Eurasia (45°E–135°E, 55°N–75°N) in the NH and the Antarctic Peninsula region (270°E–315°E, 50°S–80°S), as well as the rest of Antarctica (0°E–270°E, 55°S–90°S) in the SH, we calculated daily local indices using GPH and SAT anomalies. The periods of strong tropospheric responses to SPV weakening events—days 0–30 for the NH and days 30–60 for the SH—were chosen. During the first 30 days after the onset of the NH SPV weakening event, cold anomalies persisted in the Eurasian region (Supplementary Fig. S2a). Specifically, minimum peaks

of the temperature anomaly were observed on day 7 and day 22, respectively. To explain the temperature fluctuation, we included the variation of the tropospheric GPH anomalies averaged over Eurasia (Supplementary Fig. S2b). The tropospheric GPH anomalies exhibited a temporal pattern similar to the SAT anomalies, with the minimum low-pressure anomaly observed about two or three days before the minimum temperature peak. The deepening of the low-pressure circulation over Eurasia could provide a favourable condition for south-eastward cold air advection over the Eurasian region, leading to negative SAT anomalies (Lehtonen & Karpechko 2016). The evolution of lower stratospheric circulation averaged over Eurasia showed similar fluctuation with the tropospheric circulation, with correlation coefficients of 0.74, which are significant at the 95% confidence level. This result suggests a possibility that the lower stratospheric variation is linked to the tropospheric circulation over Eurasia, which leads to the fluctuation of Eurasian

temperature. The same analysis was performed for the SH (Supplementary Fig. S3). During days 30–60, cold anomalies were prominent over the Antarctic Peninsula region, while warm anomalies were prominent over the rest of the Antarctic continent (Supplementary Fig. S3a, b). The temperature anomalies between the two regions exhibited a nearly opposite fluctuation, with a significant correlation coefficient of −0.44 at the 95% confidence level. From day 45 onwards, warming in the west and east Antarctic region and cooling in the Antarctic Peninsula region persisted without a large fluctuation. During this period, the tropospheric GPH anomaly pattern averaged over West and East Antarctica was significantly positive (Supplementary Fig. S3c). The high-pressure anomaly over West and East Antarctica helps provide cold air from the Antarctic continental interior through the Weddell Sea to the Antarctic Peninsula region, leading to negative anomalies, while over the rest of Antarctica, the northerly circulation anomaly brings warm air from the eastern Weddell Sea to eastern Antarctica, resulting in robust positive SAT anomalies (Kwon et al. 2020). The evolution of lower stratospheric circulation averaged over West and East Antarctica showed similar temporal evolution with the tropospheric circulation, with correlation coefficients of 0.8, which are significant at the 95% confidence level. This result indicates a potential link from the lower stratospheric circulation to the tropospheric circulation associated with Antarctic SAT anomalies.

We then examined the linear relationship between SAT and SPV intensity in the three calendar months after the mean onset of SPV weakening events for each hemisphere (Supplementary Fig. S4; this figure is similar to Fig. 3, except for the relationship between SAT and the SPV during the calendar months). The selected months began with the first month following the mean onset date of the SPV weakening events in each hemisphere. This was chosen because polar stratospheric anticyclonic anomalies experienced the greatest development in both hemispheres during the first month after an SPV weakening event occurred (Figs. 4, 5). The trends in SAT anomalies and the SPVI were removed prior to calculation. In the NH, when the February SPV weakened, surface cooling occurred over Eurasia and warming occurred over north-eastern North America from February to April, especially in March and April. However, in February, surface temperatures and the SPVI were not significantly correlated. In the SH, when the October SPV weakened, surface temperature response was greatest in November, with a significant positive correlation in the West Antarctic sector and part of East Antarctica but a significant negative correlation in the Weddell Sea. Notably, in October, a negative SAT response to SPV weakening was
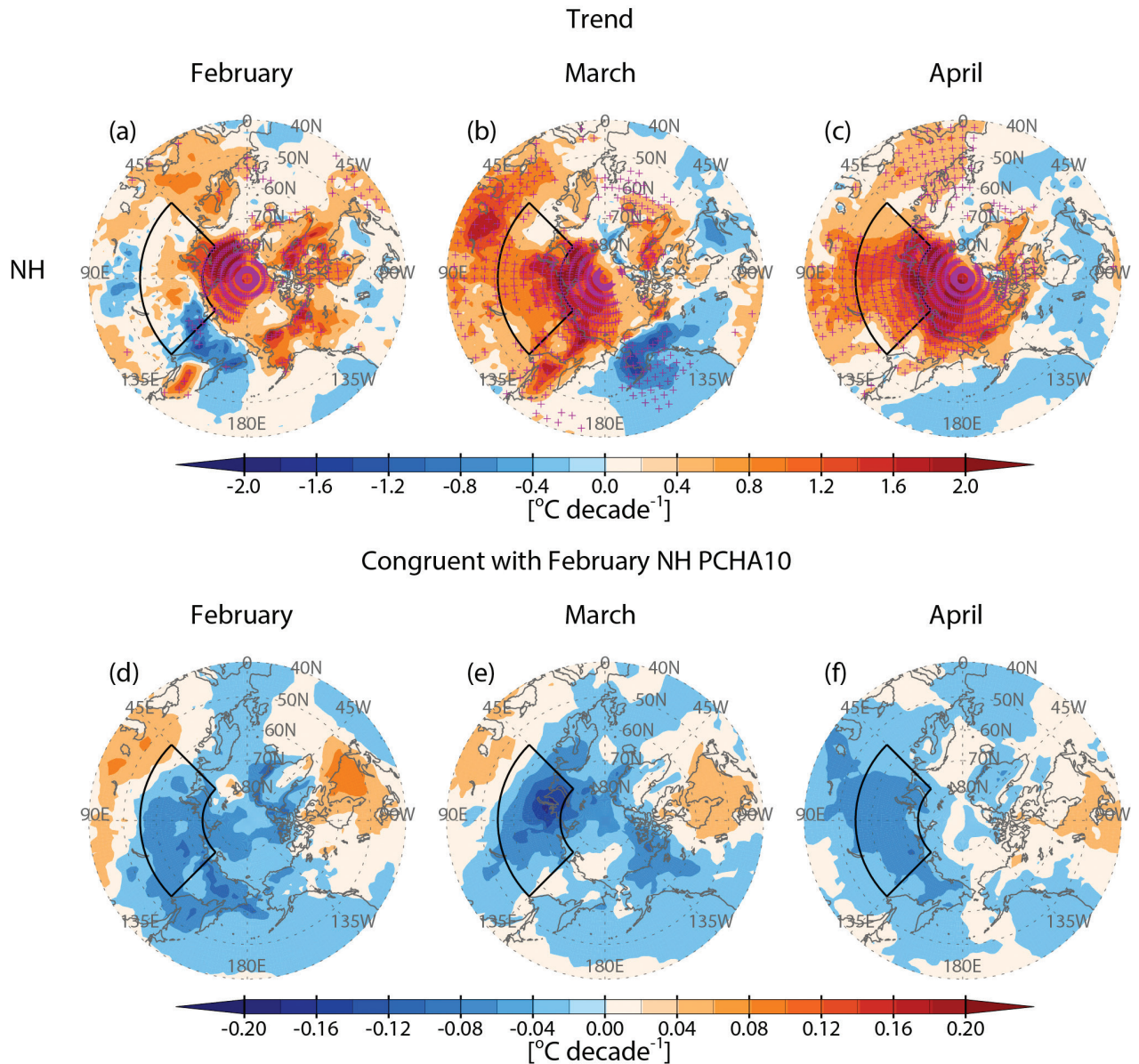
observed in the Antarctic Peninsula. In December, the relationship persisted but to a mitigated degree.

Finally, we examined the extent to which SPV weakening events contributed to the SAT trend between 1979 and 2017. In both hemispheres, the SPV weakening trend over high-latitude regions appeared to be relatively more pronounced during the first month following the mean onset date of the SPV weakening events, rather than the second and third months (Supplementary Fig. S5). Note that, in this study, we diagnosed the strength and variability of the SPV using the SPVI10. This means that we focused on the surface response based on the zonal-mean state of the SPV, despite zonal asymmetries in the SPV variability. Figure 7 illustrates the overall SAT trend, which is linearly congruent with the SPVI trend in the NH. During the analysis period, a positive SAT trend over the Arctic was prominent for all months considered. In March and April, a warming trend was observed over Eurasia. In February, the degree of surface warming was smaller, and a cooling trend was observed over central Eurasia and eastern Siberia. The congruent temperature by the SPVI trend showed negative trends, especially over Eurasia, which may partially explain the actual SAT change in February. However, the colour scale of the congruent temperature trend was one-tenth of the actual SAT trend. Overall, the SPV change in the NH did not explain the observed temperature change during the analysed period.

Figure 8 is identical to Fig. 7, except for the SH. Between 1979 and 2017, the SAT increased over East Antarctica, the Weddell Sea and the Amundsen–Ross seas in October. In November, the positive SAT change was similar to that in October but mitigated by cooling over the Antarctic Peninsula. Additionally, in December, a slight but insignificant cooling trend was observed over Antarctica, except for the Antarctic Peninsula, where significant cooling was observed. This congruent temperature pattern illustrates the SAT trend in October and November, including the warming trend over East Antarctica and the cooling trend over the Antarctic Peninsula. However, as in the NH, the degree to which the congruent temperature trend correlates with the SPVI trend was much lower than the actual temperature change in the SH, indicating that the long-term SAT trend is only partially explained by the change in the SPV on the basis of the observational analysis.

Discussion

Our results show that in the SH, the onset dates of SPV weakening events are concentrated in the austral spring season, whereas in the NH, they occur over a longer time span, from the boreal autumn to the following spring

Trend

February   March   April

NH

$[^\circ C\ \text{decade}^{-1}]$

Congruent with February NH PCHA10

February   March   April

$[^\circ C\ \text{decade}^{-1}]$

Fig. 7 Spatial distributions of (a–c) trend in the SAT anomaly and (d–f) trend in the SAT anomaly linearly congruent with NH SPVI (February NH PCHA10). Results are shown for (a, d) February, (b, e) March and (c, f) April in the NH. Pink crosses in (a–c) indicate significant values at the 95% confidence level. Linear trends in the SAT anomaly and NH SPVI were removed before calculating the regression map. Black solid boxes mark the Eurasia region (45°E–135°E, 55°N–75°N).

(Table 1). This suggests that the impact of NH SPV weakening events could occur over a period of almost half a year, from November to March. However, surface influence in the SH is more pronounced during certain seasons than in the NH, as SPV weakening events are mainly confined to spring (Figs. 1, 2). The SPV in both hemispheres is largely disturbed by an increase in wave forcing from the troposphere (Choi et al. 2019; Kwon et al. 2020). In the SH, the maximum wave activity in the winter (July–August) is

weaker than that in the NH winter (December–February) and is limited to October and November. In contrast, in the NH, strong wave forcing occurs over half a year, from boreal autumn to the following spring (Graversen & Christiansen 2003). The difference in the strength and annual cycle of wave forcing from the troposphere between the NH and SH likely contributes to the difference in the onset date coverage of SPV weakening events between the two hemispheres.

Trend

October

November

December

Congruent with October SH PCHA10

October
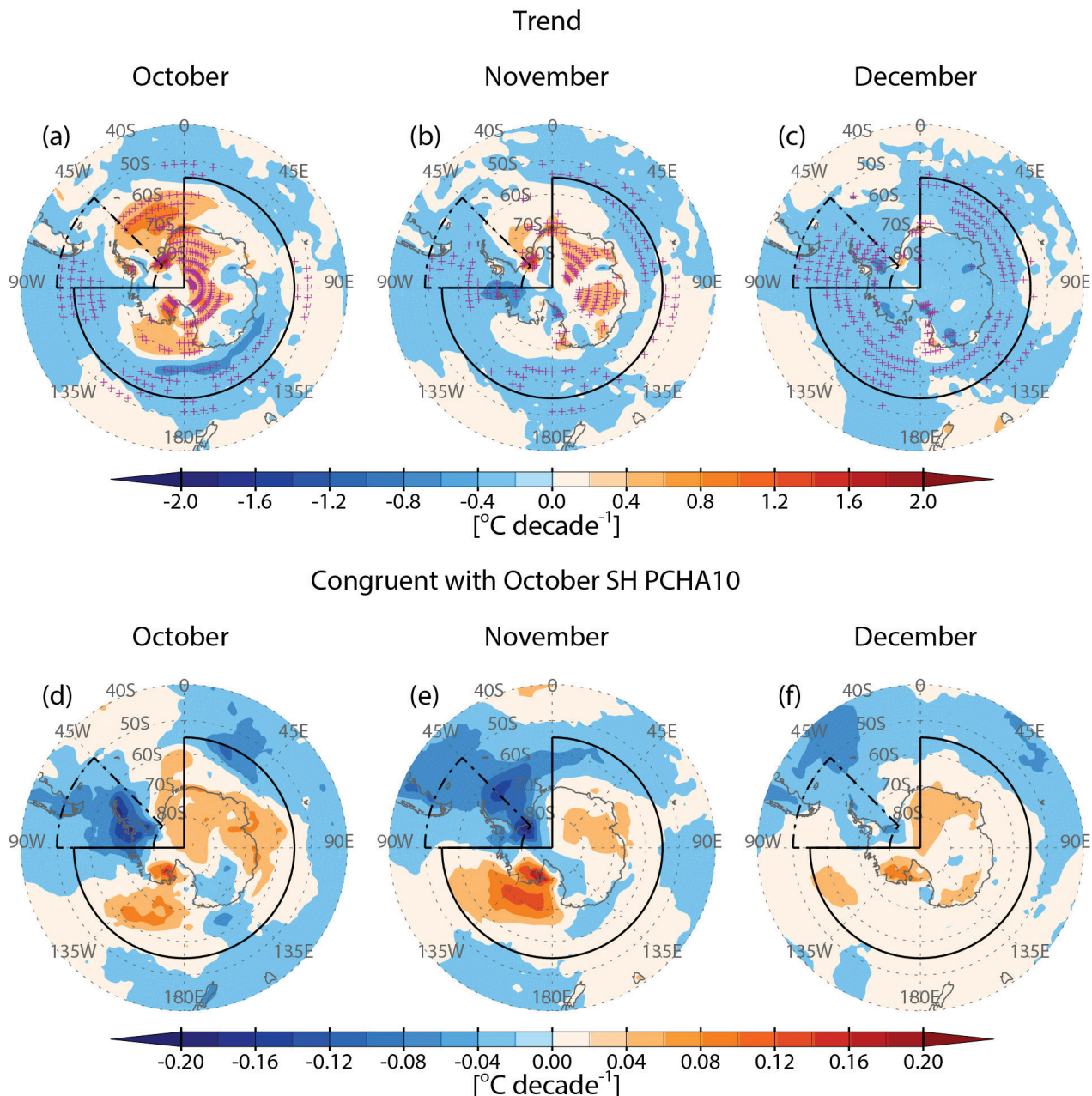
November

December

Fig. 8 Spatial distributions of (a–c) trend in the SAT anomaly and (d–f) trend in SAT anomaly linearly congruent with the SH SPVI (October SH PCHA10). Results are shown for (a, d) October, (b, e) November and (c, f) December in the SH. Pink crosses indicate significant values at the 95% confidence level in (a–c). Linear trends in the SAT anomaly and SH SPVI were removed before calculating the regression map. Black dashed-dotted and black solid boxes indicate the Antarctic Peninsula region (270°E–315°E, 50°S–80°S) and the rest of Antarctica (0°E–270°E, 55°S–90°S), respectively.

Another notable result of this study is that SPV weakening events in the NH occurred more frequently in December and February before 2000 and more frequently in January after 2000 (Table 1, Supplementary Fig. S6). Kim et al. (2014) showed that the decreased sea-ice cover in November and December over the Barents–Kara seas in recent decades likely leads to the weak polar vortex during mid-winter in the NH via enhancement of the upward propagation of planetary-scale waves. According to Cohen, Furtado et al. (2014), high October snow cover is associated with a weak polar vortex in the stratosphere at the end of December through mid-to late January as a result of an increase in heat flux into the lower stratosphere. Supplementary Fig. S7 shows the sea-ice cover

anomaly averaged over November and December over the Barents–Kara seas (30°E–90°E, 70°N–80°N) and the October Eurasian SCE anomaly. The October Eurasian SCE anomaly is normalized by a standard deviation for October from 1979 to 2017 (1.98×10^6 km^2). Similar analyses were conducted by Kim et al. (2014) and Cohen et al. (2012), but here we present updated versions. We found a significant decrease in the sea-ice cover anomaly and an increase in the SCE anomaly. Examining whether there is a difference in meridional eddy heat flux before and after 2000, we found that after 2000 heat flux anomalies increased starting from mid-November through mid-to late January (Supplementary Fig. S8). This contrasts with the period before 2000, when positive heat flux anomalies were observed from mid-November to early December and from mid- to late February. The positive heat flux anomaly was associated with strong upward wave propagation from the troposphere to the stratosphere before the weak SPV events. Therefore, the different behaviour in meridional eddy heat flux anomalies linked to early-winter sea-ice cover over the Barents–Kara seas and the October Eurasian SCE could explain the difference in the NH SPV strength between the two periods. Other factors, including the Madden-Julian Oscillation and sea-surface temperature, might also contribute to SPV variability (Garfinkel et al. 2012; Garfinkel et al. 2015; Zhang et al. 2016; Wang et al. 2023)

In the SH, however, SPV weakening events tend to occur during September and October regardless of the time period (Supplementary Fig. S9), but they have occurred more frequently since 2000 (Kwon et al. 2020; Table 1). The ozone concentration over Antarctica—which has increased in recent years because of the Montreal Protocol (Banerjee et al. 2020)—has contributed substantially to SPV variability (Thompson & Solomon 2002). However, Kwon et al. (2020) showed that the more frequent occurrences of SPV weakening events in the SH since the 2000s were likely primarily influenced by strong upward wave propagation from the troposphere to the stratosphere rather than by ozone recovery. Further research on the differences observed in the temporal distribution of SPV weakening events in the NH and their frequency in the SH since the 2000s is required to fully understand their causes.

Although we observed downward propagation of positive PCH anomalies from the stratosphere to the troposphere in both hemispheres, the persistence of the surface response and the timing at which the surface response occurred were different (Figs. 1a, 2a). After SPV weakening events, the lower stratospheric and tropospheric anomalies lasted up to about 60 days in the NH as opposed to ca. 90 days in the SH. The persistent differences between the two hemispheres were reported by Thompson et al. (2005). In the NH, SPV weakening

events and surface responses occurred almost simultaneously, whereas a time lag of approximately one month was observed in the downward impact of the SPV weakening events in the SH. This is consistent with the tendency for the negative annular mode after SPV weakening events to occur more frequently during the first month in the NH, but more often one month later in the SH (Supplementary Fig. S1). Recent studies have noted a delayed surface response to an SPV weakening event that occurred in 2019 in the SH, suggesting a potential link to factors such as the Indian Ocean Dipole or ozone concentrations (Lim et al. 2020; Lim et al. 2021; Jucker & Goyal 2022). Figure 2a suggests that the delayed surface response in the SH tends to be more frequent after SPV weakening events than that in the NH, which has important implications for the predictive skill of current seasonal forecasting systems. Further studies are required to understand the factors that interact with downward coupling following SPV weakening events in the SH.

According to our results, the weakening of the SPV in the NH led to colder temperatures over Eurasia and north-eastern North America for up to 30 days after onset. However, in the SH, SPV weakening events resulted in warming in East Antarctica and cooling in the Antarctic Peninsula 30 days onwards after onset. Atmospheric circulation anomalies via stratosphere–troposphere downward coupling after SPV weakening events are related to the surface temperature responses for each hemisphere. However, the congruency of the surface temperature trend according to the SPV trend appeared to be small in both hemispheres. We confirmed the weakening of vortices in the NH in winter and the SH in early spring, which have been reported previously (Hu et al. 2005; Hu & Pan 2009; Fu et al. 2010; Alexeev et al. 2012; Bohlinger et al. 2014; Garfinkel et al. 2017; Seviour 2017; Kretschmer, Coumou et al. 2018; Kwon et al. 2020). The weakening of polar vortices has coincided with recent Arctic Amplification (Cohen, Screen et al. 2014) and Arctic sea-ice loss (Kim et al. 2014). However, these trends are not significant in either hemisphere owing to fluctuating trends between 1979 and 2017. Sometimes, the positive trend offsets in the opposite negative direction on decadal timescales, occurred around 2000 (Hu et al. 2018; Hu & Guan 2018; Supplementary Figs. S10, S11). Additionally, there is high interannual variability (Langematz & Kunze 2006). In the SH, the trends in temperature and circulation resulting from ozone recovery in the 21st century are generally opposite to those caused by ozone losses, including a weakening of the SH SPV (Banerjee et al. 2020; Zambri et al. 2021). However, the magnitude of the trends while ozone levels were increasing was smaller than that while ozone levels were decreasing (Banerjee et al. 2020; Zambri et al.

2021). Additionally, higher levels of greenhouse gases can counteract the influence of ozone by strengthening the polar vortex (Banerjee et al. 2020; Rao & Garfinkel 2021). Therefore, in the SH, the insignificant contribution of ozone recovery and the opposing effects of greenhouse gases increase on SPV weakening are likely to mitigate the long-term trend of the polar vortex intensity. Consequently, the weaker trend of the SPV weakening may result in only slight congruency even if the linear relationship between SPV intensity and SAT is considerable (Supplementay Fig. S4). In addition, because SAT is known to be affected by other factors such as tropical forcing, natural variability, topographic layout and sea-ice loss (Cohen, Screen et al. 2014; Rahaman et al. 2019; England et al. 2020; Jun et al. 2020), SPV weakening may not fully explain SAT trends. Detailed examinations are necessary to improve our understanding of the impacts of SPV change on surface weather patterns.

The observed number and decadal variability of weak SPV events may be affected by different detection methods. For example, defining weak SPV events based on zonal-mean zonal wind diagnostics at one latitude yields zero events during the early to mid-1990s in the NH (Charlton & Polvani 2007; Butler et al. 2015). However, utilizing PCH anomalies classifies a similar number of weak NH SPV events during the 1990s, as are observed in other decades (Table 1). Using different data sets is also related to the sampling issue (Butler et al. 2015). Consequently, the use of different definitions may result in some distinctions in composite features of stratosphere–troposphere coupling and tropospheric response, such as timing or intensity. We examined the possibility that different definitions of polar vortex strength in the NH might have influenced composite results of stratosphere–troposphere coupling and tropospheric responses. The fourth and fifth columns in Table 1 show NH SSWs based on the wind reversal method. The onset date of the SSWs is defined as the first day when the zonal-mean zonal wind (U) reverses from westerly to easterly at 10 hPa and 60°N during the boreal winter (November–March; Choi et al. 2019). During the analysis period, a total of 24 SSWs occurred, with an average onset date of 1 February, which is about two weeks later than the average onset date of NH weak SPV events obtained based on the PCH anomalies. Out of 22, 16 SPV weakening events in the NH are identified as SSWs. We detected 11 SSW events before 2000 and 13 SSWs after 2000, indicating that there is no large difference in frequency between the two periods. We reconducted composite analysis using SSWs from the method of wind reversal (Supplementary Figs. S12, S13, S14) and compared those with Figs. 1a, b, 3a–c and Supplementary Fig. S6. They showed similar features. This comparison supports that, at the very least, the main results in composite reanalysis in this study are not largely affected by different definitions. Forming a consensus for standardized definitions of events is ongoing and beyond the scope of this study. We focus on reviewing and examining the relationship between SPV variability and surface responses in recent decades.

Conclusion

In this study, we used ERA-Interim reanalysis data to investigate SPV trends for a 39-year observation period in both hemispheres and attempted to determine when the coupling between the stratosphere and troposphere was strongest. As SSWs are rare in the SH, we introduced and defined SPV weakening events as occurrences when PCH anomalies at 10 hPa were higher than the 95th percentile, which corresponds to 1.73 in the NH and 1.65 in the SH. Since 2000, SPV weakening events have occurred more frequently in the SH, whereas in the NH, a similar number of SPV weakening events have occurred both before and after 2000. In both hemispheres, the SPV showed a small weakening trend. Furthermore, the onset of annual SPV weakening occurred in mid-January in the NH and in late September in the SH. After the onset of SPV weakening events, stratosphere and troposphere coupling occurred rather quickly in the NH, where the relationship between stratospheric PCH anomalies and tropospheric PCH anomalies was prominent within the first 30 days. However, in the SH, the coupling occurred approximately 30–90 days after onset. Moreover, in the NH, the influence of the stratosphere on the troposphere occurred over a longer time span, from November to March, but in the SH, stratospheric influence was confined to a narrow time band from October to November.

In the NH, significant and non-significant—but still observable—cold anomalies occurred over northern Eurasia and north-eastern North America, respectively, within 30 days after the onset of SPV weakening events. However, in the SH, over a period of 30–60 days after the onset of the SPV weakening, surface temperatures showed warming responses across Antarctica, save for the Antarctic Peninsula. These contrasting surface temperature responses to SPV weakening events in both hemispheres were due to associated changes in GPH in the troposphere, with a trough over Eurasia in the NH but a higher height anomaly over East Antarctica in the SH, both of which are reminiscent of changes in GPH in the lower stratosphere.

In our study, the relation between SPV weakening events and SAT appears to be robust, owing to a change in tropospheric circulation and subsequent air mass advection, as mentioned earlier in the text, which is reminiscent of the change in upper-level circulation. However,

the congruent temperature trend differed from the actual temperature trend in the NH and was much smaller than the actual trend in the SH, as the long-term SPV trend was rather small owing to temporal fluctuations during the analysis period.

Using a consistent detection method, we have herein reported unique differences in the anomalous behaviour of NH and SH SPV weakening events and their impacts on surface climate. The results provide a useful reference and motivation for future studies associated with improving weather forecasting, For instance, our findings can help determine when and where the strongest downward impact may occur and the nature of that impact. In addition, the differences in the persistence of the surface response and the timing at which the surface response occurred may be an intriguing issue meriting further investigation.

Acknowledgements

Disclosure statement

The authors report no conflict of interest.

Funding

References

Alexeev V.A., Esau I., Polyakov I.V., Byam S.J. & Sorokina S. 2012. Vertical structure of recent Arctic warming from observed data and reanalysis products. *Climatic Change 111*, 215–239, doi: 10.1007/s10584-011-0192-8.

Banerjee A., Fyfe J.C., Polvani L.M., Waugh D. & Chang K.L. 2020. A pause in Southern Hemisphere circulation trends due to the Montreal Protocol. *Nature 579*, 544–548, doi: 10.1038/s41586-020-2120-4.

Black R.X. & McDaniel B.A. 2007. Interannual variability in the Southern Hemisphere circulation organized by stratospheric final warming events. *Journal of the Atmospheric Sciences 64*, 2968–2974, doi: 10.1175/JAS3979.1.

Bohlinger P., Sinnhuber B.M., Ruhnke R. & Kirner O. 2014. Radiative and dynamical contributions to past and future Arctic stratospheric temperature trends. *Atmospheric Chemistry and Physics 14*, 1679–1688, doi: 10.5194/acp-14-1679-2014.

Butler A.H., Seidel D.J., Hardiman S.C., Butchart N., Birner T. & Match A. 2015. Defining sudden stratospheric warmings. *Bulletin of the American Meteorological Society 96*, 1913–1928, doi: 10.1175/BAMS-D-13-00173.1.

Byrne N.J. & Shepherd T.G. 2018. Seasonal persistence of circulation anomalies in the Southern Hemisphere stratosphere and its implications for the troposphere. *Journal of Climate 31*, 3467–3483, doi: 10.1175/JCLI-D-17-0557.1.

Charlton A.J. & Polvani L.M. 2007. A new look at stratospheric sudden warmings. Part I: climatology and modeling benchmarks. *Journal of Climate 20*, 449–469, doi: 10.1175/JCLI3996.1.

Choi H., Kim B.M. & Choi W. 2019. Type classification of sudden stratospheric warming based on pre-and post-warming periods. *Journal of Climate 32*, 2349–2367, doi: 10.1175/JCLI-D-18-0223.1.

Choi H., Kim J.-H., Kim B.M. & Kim S.J. 2021. Observational evidence of distinguishable weather patterns for three types of sudden stratospheric warming during northern winter. *Frontiers in Earth Science 9*, article no. 625868, doi: 10.3389/feart.2021.625868.

Cohen J., Agel L., Barlow M., Garfinkel C. & White I. 2021. Linking Arctic variability and change with extreme winter weather in the United States. *Science 373*, 1116–1121, doi: 10.1126/science.abi9167.

Cohen J., Furtado J.C., Jones J., Barlow M., Whittleston D. & Entekhabi D. 2014. Linking Siberian snow cover to precursors of stratospheric variability. *Journal of Climate 27*, 5422–5432, doi: 10.1175/JCLI-D-13-00779.1.

Cohen J., Pfeiffer K. & Francis J.A. 2018. Warm Arctic episodes linked with increased frequency of extreme winter weather in the United States. *Nature Communications 9*, article no. 869, doi: 10.1038/s41467-018-02992-9.

Cohen J., Screen J.A., Furtado J.C., Barlow M., Whittleston D., Coumou D., Francis J., Dethloff K., Entekhabi D., Overland J. & Jones J. 2014. Recent Arctic amplification and extreme mid-latitude weather. *Nature Geoscience 7*, 627–637, doi: 10.1038/ngeo2234.

Cohen J., Zhang X., Francis J., Jung T., Kwok R., Overland J., Ballinger T.J., Bhatt U.S., Chen H.W., Coumou D., Feldstein S., Gu H., Handorf D., Henderson G., Ionita M., Kretschmer M., Laliberte F., Lee S., Linderholm H.W., Maslowski W., Peings Y., Pfeiffer K., Rigor I., Semmler T., Stroeve J., Taylor P.C., Vavrus S., Vihma T., Wang S., Wendisch M., Wu Y. & Yoon J. 2020. Divergent consensuses on Arctic amplification influence on midlatitude severe winter weather. *Nature Climate Changge 10*, 20–29, doi: 10.1038/s41558-019-0662-y.

Cohen J.L., Furtado J.C., Barlow M.A., Alexeev V.A. & Cherry J.E. 2012. Arctic warming, increasing snow cover and widespread boreal winter cooling. *Environmental Research Letters 7*, article no. 014007, doi: 10.1088/1748-9326/7/1/014007.

Dee D.P., Uppala S.M., Simmons A.J., Berrisford P., Poli P., Kobayashi S., Andrae U., Balmaseda M.A., Balsamo G., Bauer P., Bechtold P., Beljaars A.C.M., van de Berg L., Bidlot J., Bormann N., Delsol C., Dragani R., Fuentes M., Geer A.J., Haimberger L., Healy S.B., Hersbach H., Hólm

E.V., Isaksen L., Kållberg P., Köhler M., Matricardi M., McNally A.P., Monge-Sanz B.M., Morcrette J.-J., Park B.-K., Peubey C., de Rosnay P., Tavolato C., Thépaut J.-N. & Vitart F. 2011. The ERA-Interim reanalysis: configuration and performance of the data assimilation system. *Quarterly Journal of the Royal Meteorological Society 137*, 553–597, doi: 10.1002/qj.828.

England M.R., Polvani L.M. & Sun L. 2020. Robust Arctic warming caused by projected Antarctic sea ice loss. *Environmental Research Letters 15*, 104005, doi: 10.1088/1748-9326/abaada.

Francis J.A. & Vavrus S.J. 2012. Evidence linking Arctic amplification to extreme weather in mid-latitudes. *Geophysical Research Letters 39*, article no. L06801, doi: 10.1029/2012GL051000.

Fu Q., Solomon S. & Lin P. 2010. On the seasonal dependence of tropical lower-stratospheric temperature trends. *Atmospheric Chemistry and Physics 10*, 2643–2653, doi: 10.5194/acp-10-2643-2010.

Garfinkel C.I., Feldstein S.B., Waugh D.W., Yoo C. & Lee S. 2012. Observed connection between stratospheric sudden warmings and the Madden-Julian Oscillation. *Geophysical Research Letters 39*, article no. L18807, doi: 10.1029/2012GL053144.

Garfinkel C.I., Hurwitz M.M. & Oman L.D. 2015. Effect of recent sea surface temperature trends on the Arctic stratospheric vortex. *Journal of Geophysical Research—Atmospheres 120*, 5404–5416. doi: 10.1002/2015JD023284.

Garfinkel C.I., Son S.W., Song K., Aquila V. & Oman L.D. 2017. Stratospheric variability contributed to and sustained the recent hiatus in Eurasian winter warming. *Geophysical Research Letters 441*, 374–382, doi: 10.1002/2016GL072035.

Graversen R.G. & Christiansen B. 2003. Downward propagation from the stratosphere to the troposphere: a comparison of the two hemispheres. *Journal of Geophysical Research—Atmospheres 108*, article no. 4780, doi: 10.1029/2003JD004077.

Hirano S., Kohma M. & Sato K. 2016. A three-dimensional analysis on the role of atmospheric waves in the climatology and interannual variability of stratospheric final warming in the Southern Hemisphere. *Journal of Geophysical Research—Atmospheres 121*, 8429–8443. doi: 10.1002/2015JD024481.

Hu D. & Guan Z. 2018. Decadal relationship between the stratospheric Arctic vortex and Pacific decadal oscillation. *Journal of Climate 31*, 3371–3386, doi: 10.1175/JCLI-D-17-0266.1.

Hu D., Guan Z., Tian W. & Ren R. 2018. Recent strengthening of the stratospheric Arctic vortex response to warming in the central North Pacific. *Nature Communications 9*, article no. 1697, doi: 10.1038/s41467-018-04138-3.

Hu Y. & Pan L. 2009. Arctic stratospheric winter warming forced by observed SSTs. *Geophysical Research Letters 36*, article no. L11707, doi: 10.1029/2009GL037832.

Hu Y., Tung K.K. & Liu J. 2005. A closer comparison of early and late-winter atmospheric trends in the Northern Hemisphere. *Journal of Climate 18*, 3204–3216, doi: 10.1175/JCLI3468.1.

Huang J., Hitchcock P., Maycock A.C., McKenna C.M. & Tian W. 2021. Northern Hemisphere cold air outbreaks are more likely to be severe during weak polar vortex conditions. *Communications Earth & Environment 2*, article no. 147, doi: 10.1038/s43247-021-00215-6.

Huang J., Tian W., Gray L.J., Zhang J., Li Y., Luo J. & Tian H. 2018. Preconditioning of Arctic stratospheric polar vortex shift events. *Journal of Climate 31*, 5417–5436. doi: 10.1175/JCLI-D-17-0695.1.

Jaiser R., Dethloff K., Handorf D., Rinke A. & Cohen J. 2012. Impact of sea ice cover changes on the Northern Hemisphere atmospheric winter circulation. *Tellus Series A 64*, article no. 11595, doi: 10.3402/tellusa.v64i0.11595.

Jucker M. & Goyal R. 2022. Ozone-forced Southern Annular Mode during Antarctic stratospheric warming events. *Geophysical Research Letters 49*, e2021GL095270, doi: 10.1029/2021GL095270.

Jun S.-Y., Kim J.-H., Choi J., Kim S.J., Kim B.M. & An S.-I. 2020. The internal origin of the west–east asymmetry of Antarctic climate change. *Science Advances 6*, eaaz1490, doi: 10.1126/sciadv.aaz1490.

Kidston J., Scaife A. & Hardiman S. 2015. Stratospheric influence on tropospheric jet streams, storm tracks and surface weather. *Nature Geoscience 8*, 433–440, doi: 10.1038/ngeo2424.

Kim B.M., Son S.W., Min S.K., Jeong J.H., Kim S.J., Zhang X., Shim T. & Yoon J.H. 2014. Weakening of the stratospheric polar vortex by Arctic sea-ice loss. *Nature Communications 5*, article no. 4646, doi: 10.1038/ncomms5646.

Kim S.J. & Choi H. 2021. Role of polar vortex weakening in cold events in central Asia during late winter. *Polar Science 30*, article no. 100640. doi: 10.1016/j.polar.2021.100640.

Kretschmer M., Cohen J., Matthias V., Runge J. & Coumou D. 2018. The different stratospheric influence on cold-extremes in Eurasia and North America. *NPJ Climate and Atmospheric Science 1*, article no. 44, doi: 10.1038/s41612-018-0054-4.

Kretschmer M., Coumou D., Agel L., Barlow M., Tziperman E. & Cohen J. 2018. More-persistent weak stratospheric polar vortex states linked to cold extremes. *Bulletin of the American Meteorological Society 99*, 49–60, doi: 10.1175/BAMS-D-16-0259.1.

Kwok R. & Comiso J.C. 2002. Spatial patterns of variability in Antarctic surface temperature: connections to the Southern Hemisphere annular mode and the Southern Oscillation. *Geophysical Research Letters 29*, 50–51, doi: 10.1029/2002GL015415.

Kwon H., Choi H., Kim B.M., Kim S.W. & Kim S.J. 2020. Recent weakening of the southern stratospheric polar vortex and its impact on the surface climate over Antarctica. *Environmental Research Letters 15*, article no. 094072, doi: 10.1088/1748-9326/ab9d3d.

Langematz U. & Kunze M. 2006. An update on dynamical changes in the Arctic and Antarctic stratospheric polar vortices. *Climate Dynamics 27*, 647–660, doi: 10.1007/s00382-006-0156-2.

Lehtonen I. & Karpechko A.Y. 2016. Observed and modeled tropospheric cold anomalies associated with sudden stratospheric warmings. *Journal of Geophysical Research—Atmospheres 121*, 1591–1610, doi: 10.1002/2015JD023860.

Lim E.P., Hendon H.H., Butler A.H., Garreaud R.D., Polichtchouk I., Shepherd T.G., Scaife A., Comer R., Coy L., Newman P.A., Thompson D.W.J. & Nakamura H. 2020. The 2019 Antarctic sudden stratospheric warming. *SPARC Newsletter 54*, 10–13.

Lim E.P., Hendon H.H., Shi L., de Burgh-Day C., Hudson D., King A., Trewin B., Griffiths M. & Marshall A. 2021. Tropical forcing of Australian extreme low minimum temperatures in September 2019. *Climate Dynamics 56*, 3625–3641, doi: 10.1007/s00382-021-05661-8.

Lim E.P., Hendon H.H. & Thompson D.W.J. 2018. On the seasonal evolution and impacts of stratosphere–troposphere coupling in the Southern Hemisphere. *Journal of Geophysical Research—Atmospheres 123*, 12002–12016, doi: 10.1029/2018JD029321.

Manney G.L., Butler A.H., Lawrence Z.D., Wargan K. & Santee M.L. 2022. What's in a name? On the use and significance of the term "polar vortex." *Geophysical Research Letters 49*, e2021GL097617, doi: 10.1029/2021GL097617.

Ogawa F., Omrani N.-E., Nishii K., Nakamura H. & Keenlyside N. 2015. Ozone-induced climate change propped up by the Southern Hemisphere oceanic front. *Geophysical Research Letters 42*, 10056–10063, doi: 10.1002/2015GL066538.

Polvani L.M., Waugh D.W., Correa G.J.P. & Son S.-W. 2011. Stratospheric ozone depletion: the main driver of twentieth-century atmospheric circulation changes in the Southern Hemisphere. *Journal of Climate 24*, 795–812, doi: 10.1175/2010JCLI3772.1.

Rahaman W., Chatterjee S., Ejaz T. & Thamban M. 2019. Increased influence of ENSO on Antarctic temperature since the Industrial Era. *Scientific Reports 9*, article no. 6006, doi: 10.1038/s41598-019-42499-x.

Rao J. & Garfinkel C.I. 2021. Projected changes of stratospheric final warmings in the Northern and Southern hemispheres by CMIP5/6 models. *Climate Dynamics 56*, 3353–3371, doi: 10.1007/s00382-021-05647-6.

Rao J., Garfinkel C.I. & White I.P. 2020. Predicting the downward and surface influence of the February 2018 and January 2019 sudden stratospheric warming events in subseasonal to seasonal (S2S) models. *Journal of Geophysical Research—Atmospheres 125*, e2019JD031919, doi: 10.1029/2019JD031919.

Seviour W.J. 2017. Weakening and shift of the Arctic stratospheric polar vortex: internal variability or forced response? *Geophysical Research Letters 44*, 3365–3373, doi: 10.1002/2017GL073071.

Sheshadri A., Plumb R.A. & Domeisen D.I.V. 2014. Can the delay in Antarctic polar vortex breakup explain recent trends in surface westerlies? *Journal of the Atmospheric Sciences 71*, 566–573, doi: 10.1175/JAS-D-12-0343.1.

Solomon S., Ivy D.J., Kinnison D., Mills M.J., Neely R.R. III & Schmidt A. 2016. Emergence of healing in the Antarctic ozone layer. *Science 353*, 269–274, doi: 10.1126/science.aae0061.

Sun L., Chen G. & Robinson W.A. 2014. The role of stratospheric polar vortex breakdown in Southern Hemisphere climate trends. *Journal of the Atmospheric Sciences 71*, 2335–2353, doi: 10.1175/JAS-D-13-0290.1.

Thompson D.W.J., Baldwin M.P. & Solomon S. 2005. Stratosphere–troposphere coupling in the Southern Hemisphere. *Journal of the Atmospheric Sciences 62*, 708–715, doi: 10.1175/JAS-3321.1.

Thompson D.W.J. & Solomon S. 2002. Interpretation of recent Southern Hemisphere climate change. *Science 296*, 895–899, doi: 10.1126/science.1069270.

Thompson D.W.J., Solomon S., Kushner P.J., England M.H., Grise K.M. & Karoly D.J. 2011. Signatures of the Antarctic ozone hole in Southern Hemisphere surface climate change. *Nature Geoscience 4*, 741–749, doi: 10.1038/ngeo1296.

Thompson D.W.J. & Wallace J.M. 2000. Annular modes in the extratropical circulation. Part I: month-to-month variability. *Journal of Climate 13*, 1000–1016, doi: 10.1175/1520-0442(2000)013<1000:AMITEC>2.0.CO;2.

Wang G., Hendon H.H., Arblaster J.M., Lim E.P., Abhik S. & van Rensch P. 2019. Compounding tropical and stratospheric forcing of the record low Antarctic sea-ice in 2016. *Nature Communications 10*, article no. 13, doi: 10.1038/s41467-018-07689-7.

Wang T., Fu Q., Tian W., Liu H., Peng Y., Xie F., Tian H. & Luo J. 2023. The influence of meridional variation in north Pacific sea surface temperature anomalies on the Arctic stratospheric polar vortex. *Advances in Atmospheric Sciences 40*, 2262–2278, doi: 10.1007/s00376-022-2033-2.

Wei K., Chen W. & Huang R. 2007. Dynamical diagnosis of the breakup of the stratospheric polar vortex in the Northern Hemisphere. *Science in China Series D—Earth Sciences 50*, 1369–1379, doi: 10.1007/s11430-007-0100-2.

Woo S.H., Kim B.M. & Kug J.S. 2015. Temperature variation over East Asia during the lifecycle of weak stratospheric polar vortex. *Journal of Climate 28*, 5857–5872, doi: 10.1175/JCLI-D-14-00790.1.

Zambri B., Solomon S., Thompson D.W.J. & Fu Q. 2021. Emergence of Southern Hemisphere stratospheric circulation changes in response to ozone recovery. *Nature Geoscience 14*, 638–644, doi: 10.1038/s41561-021-00803-3.

Zhang J., Tian W., Chipperfield M.P., Xie F. & Huang J. 2016. Persistent shift of the Arctic polar vortex towards the Eurasian continent in recent decades. *Nature Climate Change 6*, 1094–1099, doi: 10.1038/nclimate3136.

Zhang X., Fu Y., Han Z., Overland J.E., Rinke A., Tang H., Vihma T. & Wang M. 2022. Extreme cold events from East Asia to North America in winter 2020/2021: comparisons, causes, and future implications. *Advances in Atmospheric Sciences 39*, 553–565, doi: 10.1007/s00376-021-1229-1.